

A large-area CMOS imager as an X-ray detector for synchrotron radiation experiments

Naoto Yagi,^{a*} Masaki Yamamoto,^b Kentaro Uesugi^a and Katsuaki Inoue^a

^aSPring-8/JASRI, 1-1-1 Kouto, Mikazuki-cho, Sayo-gun, Hyogo 679-5198, Japan, and ^bSPring-8/RIKEN, 1-1-1 Kouto, Mikazuki-cho, Sayo-gun, Hyogo 679-5148, Japan.
E-mail: yagi@spring8.or.jp

The performance of a CMOS flatpanel imager from Hamamatsu Photonics (C7942) has been tested in various synchrotron radiation experiments. This detector has a detection area of about 120 mm × 120 mm with 0.05 mm pixels, and a frame rate of 2 s⁻¹. The commercially available product was insensitive to X-rays with an energy lower than 15 keV, but slight modifications solved this problem. Images obtained in small-angle scattering, protein crystallography and medical imaging experiments were all of high quality. The fast readout and the large area are advantageous in real-time imaging. Although its noise level is higher than the area detectors that are currently used in synchrotron radiation experiments, it is particularly useful in experiments where other bulky detectors cannot be used. Its relatively low price (about USD 30000) makes it a unique option in the choice of detectors.

Keywords: CMOS detector; small-angle diffraction; medical imaging; protein crystallography; SPring-8.

1. Introduction

Solid-state digital imaging devices are widely used in synchrotron radiation experiments. The most commonly used device is a CCD (charge-coupled device) which is used in diffraction and high-resolution imaging experiments. The advantages of the CCD are (i) low noise, (ii) small pixel size (down to 3 µm) and (iii) large pixel number (up to 4000 × 4000 so far). However, the CCD has a limitation that (i) the pixel size cannot be made large (typically <30 µm), (ii) it is easily damaged by X-rays and (iii) readout is slow because of its charge-transporting method. Thus, most CCD-based X-ray detectors are those with a tapered optical fibre for crystallography (Gruner & Ealick, 1995) and those with indirect lens-coupling for high-resolution imaging (Koch *et al.*, 1998; Uesugi *et al.*, 2001) and for small-angle scattering [with an X-ray image intensifier (Amemiya *et al.*, 1995)]. Use of a tapered optical fibre tends to make CCD detectors complicated and expensive.

Owing to the high cost of CCD detectors with tapered fibres, other types of solid-state X-ray image sensors have been tested in synchrotron radiation experiments. One example is an amorphous silicon imager, which is a photodiode array with an active TFT (thin-film transistor) matrix readout. It can be very large (more than 300 mm) and its sensitivity can be enhanced by the use of amorphous selenium as a converting media of X-ray photons to elec-

trons. The TFT-based imagers are already used for medical diagnosis. However, they have limitations in spatial resolution (typically >100 µm) and high noise owing to the properties of the amorphous silicon semiconductor.

A CMOS (complementary metal-oxide semiconductor) flatpanel image sensor is also a matrix-addressed photodiode array. Compared with the TFT imager, this type of detector has the advantage that the pixel can be smaller (as small as with the CCD). Since most of the applications in synchrotron radiation experiments, especially those at third-generation facilities, require high spatial resolution, a CMOS imager seems to be a promising new technology.

We have tested a CMOS flatpanel imager from Hamamatsu Photonics in various synchrotron radiation experiments. Although the presently available product has a higher noise level than the detectors that are currently used for these experiments, its large area and low cost make the CMOS imager an attractive option in the choice of detectors.

2. Methods

CMOS flatpanel imagers are already commercially available, mainly for non-destructive testing and radiography. So far we have tested two CMOS flatpanel imagers from different manufacturers. One is the C7942 from Hamamatsu Photonics KK (Hamamatsu, Japan) and the other is the Shad-o-Box 1024 from Rad-Icon (Santa Clara, CA, USA). These imagers are quite similar in their characteristics, which are shown in Table 1. The results using the Shad-o-Box have been reported elsewhere (Yagi *et al.*, 2004).

The data presented here are those from C7942. This detector has a large (120 mm × 120 mm) active area with more than 5 × 10⁶ pixels. This large size with high resolution makes it suitable for various synchrotron experiments. Rad-Icon also produces CMOS imagers with a similar number of pixels. However, the detector from Rad-Icon is composed of eight 512 × 1024 pixel devices, while C7942 is a single device.

The C7942 imager was developed mainly for industrial non-destructive testing. Thus, its window is made of 1 mm-thick aluminium. Also, it has a 'flipped' scintillator: a layer of needle-shaped CsI:Tl crystals, with a thickness of 0.15 mm, was grown on a glass substrate and then put on the CMOS device with the CsI in contact with the device. The glass substrate, together with the carbon plate and a plastic foam to press the scintillator onto the CMOS device,

Table 1

Characteristics of the two CMOS imagers given by the manufacturers (<http://www.rad-icon.com/> and <http://www.hamamatsu.com/>).

For a comparison, data for the most widely used CCD-based detector for protein crystallography (<http://www.adsc-xray.com/>) are also shown.

	Rad-Icon Shad-o-Box 1024	Hamamatsu C7942	ADSC Quantum 4R
Number of pixels	1024 × 1024	2240 × 2368	2304 × 2304 (four CCDs)
Pixel size (µm)	48	50	82
Readout time (s)	0.44 (two channels)	0.44 (eight channels)	9
Dark current (e ⁻ pixel ⁻¹ s ⁻¹)	4000	5900	0.03
Readout noise (RMS, e ⁻)	<500	1100	10 @ 150 kHz
AD converter (bits)	12	12	16
Maximum charge (e ⁻ pixel ⁻¹)	~2 × 10 ⁶	2.2 × 10 ⁶	4.4 × 10 ⁵
Electrons per ADU	500	500	7
Electrons per X-ray photon	125 @ 15 keV†	165 @ 12.4 keV‡	8.5 @ 12.4 keV
Resolution (line-pairs mm ⁻¹)	10	8	90 µm (FWHM)
Phosphor	Gd ₂ O ₂ S:Tb	CsI:Tl	Gd ₂ O ₂ S:Tb
Operating temperature	Room temperature	Room temperature	223 K
Size (mm)	124 × 127 × 23	200 × 198 × 28	330 × 356 × 610
AD converter (bits)	12	12	16

† From the data of Yagi *et al.* (2004). ‡ Measured in the present experiments for C7942MOD.

absorbs low-energy X-rays considerably. Thus, to make the imager sensitive to X-rays below 15 keV, it was necessary to change the window to 1 mm-thick polycarbonate, and the glass substrate to a 1 mm-thick amorphous carbon plate. The modified imager is hereafter called C7942MOD.

Another, more drastic, alteration to enhance sensitivity to low-energy X-rays is to directly grow a layer of CsI crystals on the surface of the CMOS device. In this design, the only window material is a 1 mm-thick polycarbonate to insulate the CsI scintillator which is deliquescent. A prototype detector with this design was constructed. Since it was designed for low-energy X-rays, the phosphor was 0.03 mm-thick. This is referred to as C7942HR in this report.

C7942 (and the other two modified imagers) has 2400×2400 pixels (pixel size $0.05 \text{ mm} \times 0.05 \text{ mm}$), but only 2240 (horizontal) \times 2368 (vertical) pixels are effective. C7942 is read out by eight charge amplifiers, each of which is connected to a one-eighth segment of the detector [$300 \text{ (H)} \times 2400 \text{ (V)}$ pixels]. In a usual setting the segments are aligned horizontally. The analogue signal is digitized by a 12-bit analogue-to-digital converter and the data are transferred to a frame grabber on a personal computer through RS422 digital connection. Two frame grabbers (IMAQ PCI-1424 from National Instruments, Austin, TX, USA and PC-DIG from Coreco Imaging, San Jose, CA, USA) were used in the present tests.

As is the case with other solid-state imaging devices, CMOS devices have defects. The data in dead pixels and defect lines (typically less than 20 lines in the entire device) were replaced by interpolation.

Experiments were carried out at three beamlines in the third-generation synchrotron radiation facility SPring-8 (Harima, Hyogo, Japan). BL40XU is a beamline specialized to deliver high flux: radiation from a helical undulator is used without monochromatization (Inoue *et al.*, 2001). Since the flux is too high for the present purpose, the X-ray intensity was reduced by closing the slits at the front end, and also by using aluminium absorbers. BL38B1 is a bending-magnet beamline equipped with a Si(111) double-crystal monochromator, a goniometer and a detector for protein crystallography. BL20B2 is a medium-length (200 m) bending-magnet beamline with a Si(311) double-crystal monochromator for imaging experiments (Goto *et al.*, 2001). The images were recorded in the downstream hutch (hutch 3) where an X-ray beam with a width larger than one side of the detector area (120 mm) was available.

3. Results

3.1. Noise and dark current

The dark current of C7942MOD increased by 7.8 ADU, *i.e.* 3900 electrons, every second at 295 K (equivalent to $0.63 \text{ fA pixel}^{-1}$). This is smaller than the nominal value of 5900 electrons (Table 1), probably because of the lower temperature.

The readout noise of the detector was estimated with C7942MOD by the following method: two blank exposures with the same exposure time were made and the difference image of the two images was calculated. Then, an area with 100 pixels \times 100 pixels that did not include a border between segments or hot pixels was selected and the standard deviation in the area was calculated. The value was divided by $2^{1/2}$ to give an estimate of the readout noise. In a 0.44 s exposure, the readout noise was estimated to be 3.34 ± 0.01 ADU (mean \pm standard deviation, $n = 5$), corresponding to 1670 electrons. This is larger than the nominal value of 1100 electrons (Table 1).

In a 10 s exposure, the estimation gave 3.45 ± 0.03 ADU ($n = 5$). Since the readout noise should be independent of the exposure time, the small increase (0.11 ADU) compared with the value in the 0.44 s

exposure is considered to be due to the fluctuation in the dark current which accumulated in the longer exposure. This result shows that, if properly subtracted, dark current does not markedly increase noise in an image.

3.2. Conversion gain

The sensitivity was studied by measuring the conversion gain, which is the number of A/D converter units created by each X-ray photon. The data points below 20 keV were obtained at BL40XU. In this experiment, a small beam (about 0.5 mm in diameter) was made by placing a lead plate with a hole within the small-angle scattering from silica particles (mean diameter 100 nm, Seahoster KE-P10, Nippon Shokubai, Kyoto, Japan). The intensity was measured using both a YAP:Ce scintillation counter (KX-101, Oken, Tokyo, Japan) and the three CMOS imagers, and the results were compared. With the imagers, the intensity within the beam was integrated after background subtraction. The flux was reduced to below $10000 \text{ counts s}^{-1}$ to avoid saturation of the scintillation counter.

Assuming 100% efficiency for the scintillation counter, C7942 was found to have a conversion gain of less than 0.1 at 15 keV (Fig. 1, open circles). This low gain is primarily due to absorption by the aluminium window and the glass substrate of the scintillator. When the detector was modified for low energies (C7942MOD), the conversion gain was about 0.5 (Fig. 1, open triangles). Each 15 keV X-ray photon should create about 1000 scintillation photons (Dorenzo & Moses, 1993). Since 0.5 ADU corresponds to 250 electrons, the net conversion gain is about 25%, assuming that each scintillation photon creates one electron in the CMOS device (the peak of scintillation of CsI:Tl, at around 540 nm, is close to 2.3 eV, which is the band gap of silicon). Considering that there is an aluminium layer to reflect the scintillation photons that are emitted towards the X-ray source, this conversion gain is less than half of that expected. Below 15 keV, the conversion gain decreases primarily because the photon energy decreases. However, the gain at 8.1 keV was only 0.17, suggesting that absorption by the carbon substrate for the scintillator is still significant.

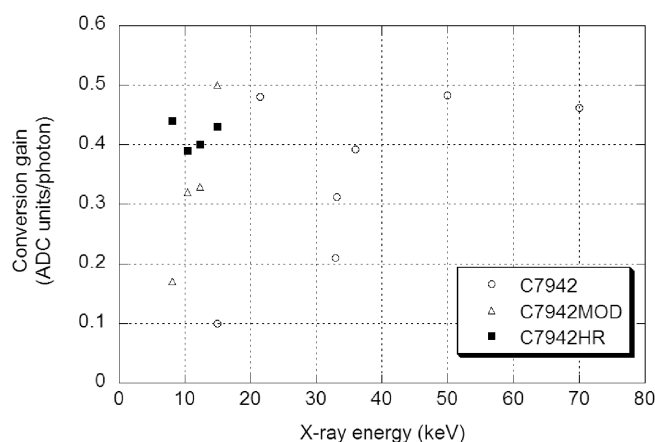


Figure 1

Conversion gain of three types of C7942. The ordinate is an average AD-converter output value created by each X-ray photon. The data points are at energies of 8.1, 10.5, 12.4, 15.0, 21.5, 33.0, 33.2, 36.0, 50.0 and 70.0 keV. The open circles were measured with C7942. The point at 15.0 keV was measured at BL40XU and calibrated with a scintillation counter. The other points for C7942 were measured at BL20B2, calibrated by an ionization chamber using mass-energy attenuation coefficients. The filled squares were measured with C7942HR and the open triangles with C4880MOD. These were measured at BL40XU and calibrated with a scintillation counter.

C7942HR, which has a 30 μm scintillator, had a conversion gain of 0.4 even at 8.1 keV (Fig. 1, filled squares), showing that the direct deposition of the scintillator is an effective method for increasing the sensitivity for low-energy X-rays. The gain was almost constant over the X-ray energy of 8 to 15 keV. This is because the absorption by the 30 μm -thick CsI, with a packing ratio of 70%, decreases from 93% to 42% when the X-ray energy increases from 8 to 15 keV, compensating each other.

The conversion gain of 0.4 ADU per X-ray photon means that the readout noise of 3.34 ADU, as measured in §3.1, is equivalent to 8.35 X-ray photons. Thus, if the detection limit is considered to be a few times higher than the readout noise, 20–40 X-ray photons are necessary to be detected as a signal. Also, since 0.4 ADU is equivalent to 200 e^- , 11 000 X-ray photons saturate a pixel which has a capacity of $2.2 \times 10^6 e^-$ (Table 1).

Conversion gain above 20 keV was measured at BL20B2 with C7942. The X-ray flux was calibrated by using an ionization chamber (S-1196B1, Oken, Tokyo, Japan) filled with air. The current in the ionization chamber was converted to X-ray flux using mass–energy attenuation coefficients (Fig. 1, open circles). Mass attenuation coefficients, which are usually used at lower energies, would give larger values for the flux. Unlike a mass attenuation coefficient, which is a simple attenuation ratio of X-rays by matter, a mass–energy attenuation coefficient deals with the transfer of energies of all primary charged particles created by X-ray photons. Thus, incoherent Compton scattering, which is significant with X-rays above 20 keV, is taken into account. The conversion gain calculated this way (Fig. 1) does not fall far below the level observed at low energies, showing that the detector is still fairly sensitive at high energies. The result also shows that the conversion gain increases above the absorption edges of Cs and I (36.0 and 33.2 keV, respectively).

The conversion gain at low energy (165 e^- per X-ray photon at 12 keV) is about 20 times larger than that in the CCD detector (8.5 e^- per X-ray photon at 12 keV, Table 1). This is because a large fraction of photons emitted by the scintillator are lost in the tapered optical fibre in the CCD detector. However, since the readout noise in the CCD detector is 1/100 of that in the CMOS detector, the low conversion gain is not a disadvantage of the CCD detector. In fact, the CCD detector has a better signal-to-noise ratio, especially when the signal is weak.

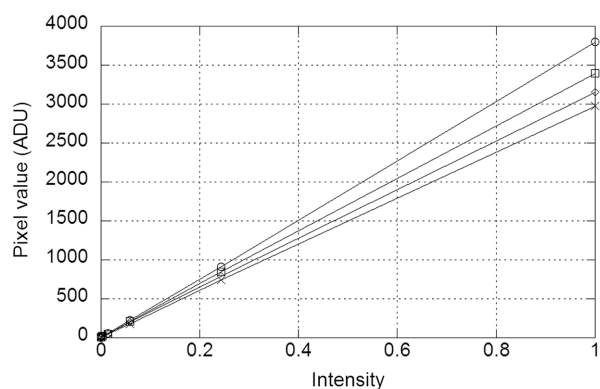


Figure 2 Linearity of sensitivity of C7942MOD. The data were obtained at BL40XU with an X-ray energy of 15.0 keV. Aluminium absorbers (0.4 mm thick) were inserted into the beam to attenuate the intensity stepwise. The intensities at four different pixels, after background subtraction, are plotted. In the ordinate, the unity of intensity was that without an absorber. For all the sets of data, the R^2 value of regression was larger than 0.9999, and the y -intercept was within 10 of the origin (the data for the regression do not include a value at the origin).

3.3. Linearity

Linearity was measured in a small-angle scattering pattern from silica particles (see above). The entire pattern was recorded with an exposure time of 2 s. 0.4 mm-thick aluminium plates were used to reduce the intensity stepwise. Four pixels that received different levels of intensity were picked up and the intensities were plotted in Fig. 2. In all four pixels, the regression coefficient is close to unity ($R^2 > 0.9999$) and the y -intercept was within 10 ADU of zero. Thus, no indication of non-linearity was found.

3.4. Spatial resolution

Spatial resolution was measured by using a resolution chart of 0.05 mm-thick lead. The slits in the chart were oriented vertically and the CTF (contrast transfer function) was measured in a horizontal section with a width of one pixel. The CTF was calculated after dark subtraction. The definition of CTF is

$$\text{CTF} = (I_{\text{bright}} - I_{\text{dark}})/(I_{\text{bright}} + I_{\text{dark}}),$$

where I_{bright} is the maximum pixel value in the area of opening of the slits and I_{dark} is that between the slits. The CTF was then converted to modulation transfer function (MTF) using the method of Coltman (1954) using the available values of the CTF.

Fig. 3 shows the result for C7942 (open diamonds), C7942MOD (open triangles) and C7942HR (filled squares). Since the pixel size is 0.05 mm, an MTF of 10 line-pairs mm^{-1} is the ultimate resolution (Nyquist frequency). The results show that 8 line-pairs mm^{-1} , which is quoted in the specification, are resolved by C7942. Better resolution is obtained with C7942HR, which is made by direct deposition of a thinner phosphor layer. The MTF does not reach unity even with very wide slits (larger than 1 mm in width), showing that the tail of a slit profile spreads to a large distance in the detector. It is likely that a low level of scintillation is scattered to some distance within the phosphor.

3.5. Non-uniformity

There is no way of illuminating the 120 mm \times 120 mm area of C7942 with a perfectly uniform X-ray field. Thus, an 18 keV beam in the third hutch of BL20B2 (300 mm horizontal, 20 mm vertical) was used and the detector was moved vertically within a 10 s exposure to

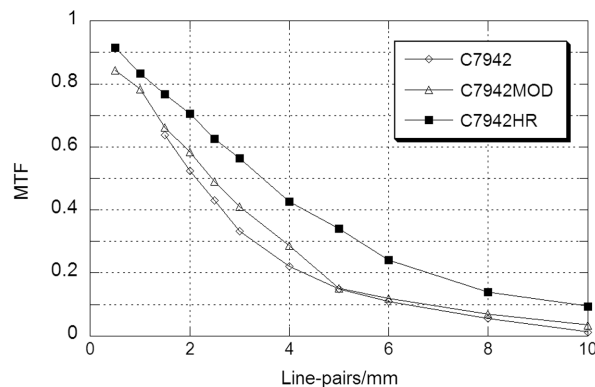


Figure 3 Modulation transfer function (MTF) for C7942 (open diamonds), C7942MOD (open triangles) and C7942HR (filled squares). A test chart made of 0.05 mm-thick lead was used. Data for C7942 were obtained at BL20B2 with an X-ray energy of 20 keV. Data for C7942HR and C7942MOD were obtained at BL40XU. A 0.05 mm gold wire was placed in the X-ray beam of 15 keV and used as a point source of fluorescent X-rays. The main energy fractions were those of $L_{\alpha 1}$ at 9.7 keV and $L_{\beta 1}$ at 11.4 keV. The data points for C7942MOD and C7942 overlap between 5 and 8 line-pairs mm^{-1} .

cover the entire detector area. Fig. 4(a) shows a vertical intensity profile after dark subtraction. Except for defect pixels, the variation in the overall response is small. When this measurement was repeated, the pixel-to-pixel variation was not reproduced, showing that it is not due to an intrinsic difference in sensitivity of each pixel. The pixel-to-pixel intensity fluctuation [standard deviation (SD) about 20 ADU] is larger than the readout noise (SD about 4 ADU). Since the pixel value was about 2000, considering that the conversion ratio is about 0.5 (Fig. 1), the number of photons recorded by each pixel was about 4000. The quantum fluctuation in the number of X-ray photons is $4000^{1/2}/4000 = 1.4\%$, which is equivalent to a fluctuation of 28 ADU. However, as pointed out by Tate *et al.* (1997), signal averaging owing to a non-zero point spread function considerably reduces this fluctuation. In the present case, based on the spatial resolution obtained in §3.4, the quantum fluctuation is expected to be only a few ADC units. Thus, half of the fluctuation is unaccounted for. One possible cause of fluctuation is the beam intensity fluctuation. Since each pixel is irradiated only for about 1 s, intensity variation at a high frequency range, for instance owing to vibration in the monochromator, may cause spatial intensity fluctuation in the recorded image.

Fig. 4(b) shows a horizontal intensity distribution, which was obtained in the same manner as Fig. 4(a) but with the detector rotated by 90°. It is similar to Fig. 4(a) but small intensity differences were found among segments, each of which is 300 pixels in width. In each segment, the response is larger by 20–30 ADU in the region closer to the origin of the horizontal coordinate.

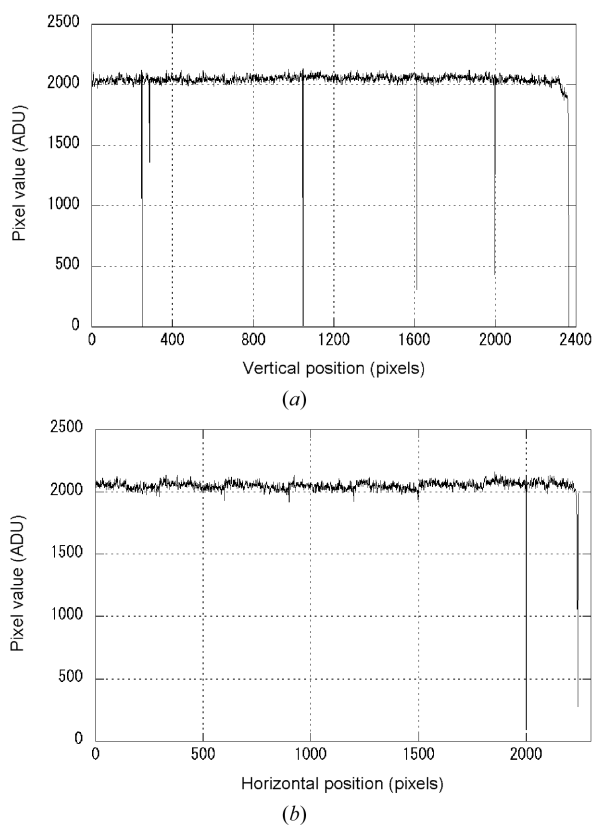


Figure 4
Flat-field response of C7942. The data were recorded at BL20B2 with an X-ray energy of 18 keV. Flat field was achieved by moving the detector across the X-ray beam that was larger than one dimension of the detector. Dark-field images were subtracted. (a) Intensity distribution along a vertical one-pixel section. (b) Intensity distribution along a horizontal one-pixel section.

Table 2
Statistics of diffraction data from a hen egg-white lysozyme crystal recorded at BL38B1 with C7942HR.

The exposure time was 5 s. The oscillation angle was 1° and 90 frames were recorded. The specimen-to-detector distance was 135 mm and the X-ray energy was 15 keV.

Space group	$P4_32_12$
Unit-cell dimensions (Å)	78.88, 78.88, 37.39 90.00, 90.00, 90.00
Resolution range (Å)	27.14–1.80 (1.86–1.80)†
Total number of reflections	58 983
Number of unique reflections	9589
Average redundancy	6.15 (4.03)†
% Completeness	84.1 (91.1)†
$R_{\text{merge}}^{\ddagger}$	0.060 (0.125)†

† In the outermost resolution range (1.86–1.80 Å). ‡ R_{merge} is defined as $\sum \sum |I(h, i) - I_{\text{av}}(h)| / \sum \sum I_{\text{av}}(h)$, where the summations are over h (for all unique reflections) and i (for all equivalent reflections). $I_{\text{av}}(h)$ is an averaged value for each unique reflection.

Table 3
 R_{merge} versus resolution.

$I/\text{sig avg}$ is the average intensity/signal for averaged reflections in the resolution range.

Resolution range (Å)	Average counts	Number observed	Number rejected	$I/\text{sig avg}$	R_{merge}
27.14–3.87	2604	2840	65	31.4	0.050
3.87–3.07	4427	3967	30	34.4	0.050
3.07–2.69	4017	6244	65	33.8	0.049
2.69–2.44	3613	7447	50	29.3	0.053
2.44–2.27	3234	7563	81	28.5	0.055
2.27–2.13	2930	7743	55	26.1	0.058
2.13–2.03	2572	7543	38	22.4	0.067
2.03–1.94	1769	6411	26	16.2	0.082
1.94–1.86	1278	5581	328	13.3	0.107
1.86–1.80	918	4090	8	9.5	0.125
27.14–1.80	2787	59 429	446	24.5	0.060

3.6. Images

Fig. 5(a) shows a small-angle X-ray diffraction pattern recorded from a dried tendon of chicken with C7942MOD. Orders of reflections from collagen fibres, which can be indexed on the fundamental period of 650 Å, can be seen. When an image obtained with the CMOS imager (Fig. 5b) was compared with an image obtained by an X-ray image intensifier with the same exposure time (Fig. 5c), the conversion gain is comparable. However, the noise level is higher with the CMOS imager.

Fig. 6 shows a diffraction pattern from a lysozyme crystal recorded using C7942 at 18.0 keV in a 15 s exposure. Strongest reflections are saturated. Diffraction patterns for further analysis were recorded from a different lysozyme crystal with C7942HR. The X-ray energy was 15.0 keV and the crystal-to-detector distance was 135 mm. In order to avoid saturation of too many reflections, the diffraction patterns were recorded in 5 s exposures. The oscillation angle was 1.0° (two oscillations). A series of 90 frames was obtained (total time required for the measurement was 15 min), and processed by the software *CrystalClear* (Rigaku MSC, Tokyo, Japan), which is based on *d*TREK* (Pflugrath, 1999). The statistics of the integrated diffraction intensities are shown in Tables 2 and 3. The overall R_{merge} value was 0.060. In the outermost resolution range (1.86–1.80 Å) where the diffraction spots are weak, the average number of photons in each spot is about 2300 from a conversion ratio of about 0.4 ADU (one unit of A/D converter output) per X-ray photon (§3.2 above). The fluctuation in the number of photons expected from Poissonian counting statistics is 2.1%, while the observed R_{merge} was as large as

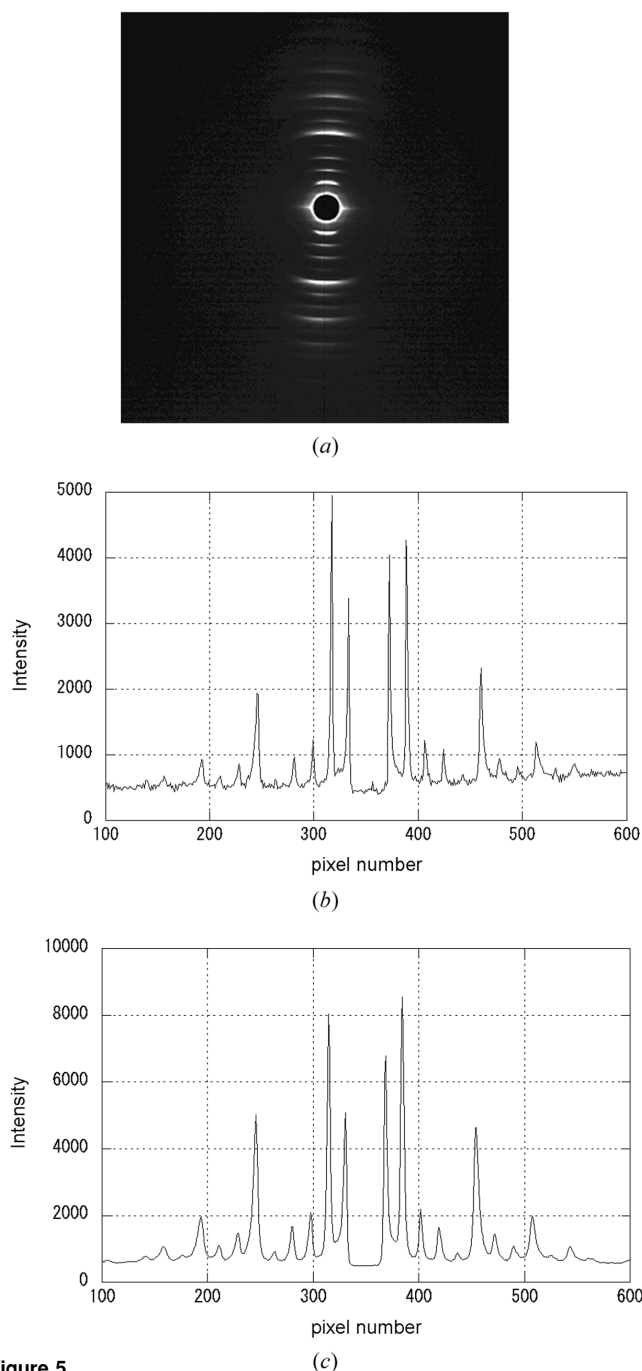


Figure 5
 An X-ray small-angle diffraction pattern from dried chicken tendon collagen at BL40XU with an X-ray energy of 15 keV. The flux was $\sim 1.0 \times 10^{11}$ counts s^{-1} . The specimen-to-detector distance was 2.8 m. (a) An image obtained by using a CMOS flatpanel detector (C7942MOD). The exposure time was 60 s. (b) Intensity distribution along the meridional axis of collagen diffraction, recorded with C7942MOD. The exposure time was 5 s. To match the spatial resolution in (c), 4×4 pixels were binned. Thus, each pixel is 0.2 mm in size. Dark current was subtracted. The profile was corrected for defect pixels. The peaks have a tail towards the higher angle because of the energy profile of the X-rays at this beamline (Inoue *et al.*, 2001). (c) The same as (b) but recorded with an X-ray image intensifier (V5445P, Hamamatsu Photonics, Hamamatsu, Japan; Amemiya *et al.*, 1995) with a 0.2 mm-thick CsI coupled to a cooled CCD camera (C4880-50-24A, Hamamatsu Photonics). An aperture number 9 was used. The intensity distribution in the region similar to that in (b) is shown. The pixel size on the detection window was about 0.22 mm. The exposure time was 5 s. Some peaks in (b) and (c) appear different in height because the sampling points of the pixels are not exactly the same in the two profiles.

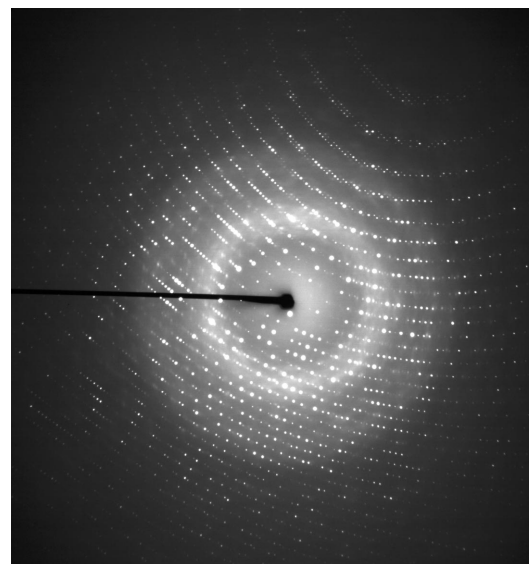


Figure 6
 An X-ray diffraction pattern from a crystal of lysozyme, which was cooled by a stream of liquid nitrogen, recorded at BL38B1 with C7942, with an exposure time of 15 s, X-ray energy of 18.0 keV, oscillation angle of 1° and specimen-to-detector distance of 80 mm. The image was processed by dark-subtraction and defect-pixel correction. Strong reflection spots are overexposed. Many spots are observed due to high mosaicity of the crystal (about 3°).

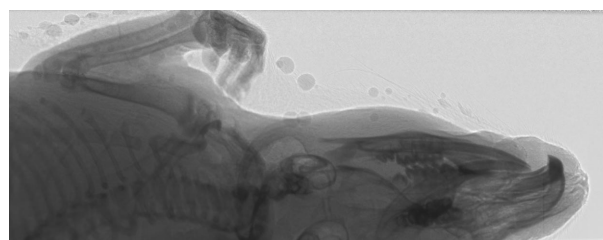


Figure 7
 Radiogram of part of the body of a euthanized rat, recorded at BL20B2 using C7942. The X-ray energy was 20.0 keV. The exposure time was 5 s with a specimen-to-detector distance of 7 m. After dark-current correction, the image was divided by an image of the direct beam to obtain uniform brightness. A sub-area with 677×262 pixels is shown. The small spheres attached to the hair are drops of water.

12.5%. Thus, the noise in the detector is significant for weak diffraction spots. This is due to the high readout noise compared with the conversion gain (Table 1). As stated in §3.2 above, the CCD detector is advantageous in measuring intensities of weak reflections. R_{merge} is larger than expected from Poissonian counting statistics, even with strong reflections in the inner resolution ranges, suggesting the presence of some systematic error in the detector.

Fig. 7 shows a radiogram of a rat. The specimen-to-detector distance was large (7 m) in order to observe an edge-enhancing effect owing to the refraction of X-rays (Yagi *et al.*, 1999). The image was recorded at about 220 m from the source point at BL20B2. The refraction induced a bright fringe around the body, and whiskers and hairs can be seen with clarity.

4. Discussion and concluding remarks

The results of the present tests show that the CMOS flatpanel detector from Hamamatsu Photonics is already a fairly mature product that can be used as an X-ray detector in synchrotron radiation experiments. In order to obtain a quantitative image, it is

necessary to correct an image for (i) non-uniformity of sensitivity, (ii) dark current, (iii) defect pixels and lines. Correction (i) is necessary only when a highly quantitative measurement is required. All these problems are common with other area detectors used in synchrotron radiation experiments. For instance, dark-current subtraction is usually carried out with CCD-based detectors, and a flat-field correction is carried out with multi-wire gas detectors. Since the non-uniformity and defect pixels are specific and invariable to each detector, the correction can be made based on calibration data. Since the dark current depends on the ambient temperature, it is recommended to record a dark image before or after each exposure.

In comparison with C7942, Shad-o-Box 1024 from Rad-Icon has a slightly better resolution (as indicated by the nominal MTF values in Table 1) and lower readout noise. However, it is susceptible to radiation damage. A permanent increase in the dark current was found after an exposure of a few Gy at 20 keV (Yagi *et al.*, 2004). On the other hand, C7942 was found to be very robust and did not show any permanent damage after irradiation of a few thousand Gy. After a very intense exposure, some afterglow of the scintillator was observed but it decayed within a few hours. These differences in sensitivity and susceptibility to radiation are related to the different designs of the two detectors. Shad-o-Box 1024, whose sensor is RadEye, is an active-pixel device, which has an amplifier in each pixel. Thus, the charge in a pixel is already amplified when it is read out. On the other hand, C7942 is a passive-pixel device without such an amplifier. It has higher noise but is robust to radiation because the amplifier is the most easily damaged part of the device.

In the design of a CMOS detector, the choice of active- or passive-pixel depends on its application. If it is only to be used with low-energy X-rays, a sufficiently thick layer of scintillator may be enough to absorb X-rays and protect the sensor. In this case, an active-pixel device is advantageous because of its lower noise. On the other hand, if the detector is for high-energy X-rays, it is necessary to employ a passive-pixel device or to introduce a fibre plate in front of the sensor to prevent X-rays from hitting the sensor. The latter design is used in commercial products (EV models from Rad-Icon and C7410 from Hamamatsu Photonics). It should be noted that an active-pixel sensor has a slightly non-linear sensitivity (Graeve & Weckler, 2001), which needs to be corrected.

Although it is a passive-pixel device, C7942 has a nominal dynamic range of 2000, which is defined as the charge capacity of a pixel divided by the readout noise. Thus, the quality of images is high enough to be used in many types of experiments. In fact, the quality of diffraction patterns from a protein crystal was high enough to be used for structural analysis (Table 2). The dynamic range can be expanded further by recording several unsaturated images and digitally adding them later. However, since there are already other detectors which give images with higher quality, C7942 will be used only when it has an advantage over such existing detectors.

Currently, the biggest advantages of the CMOS imagers in general are their compactness and low cost. At the moment, C7942 is priced at about 30000 USD, which is at least one-order lower than the price of a CCD-based detector for protein crystallography with a similar number of pixels. Since C7942 weighs less than 3 kg, it can be mounted anywhere in an experimental set-up quite easily. For instance, it can be mounted on a goniometer arm. Also, as it is only 3 cm in thickness, it can fit into a narrow space where no other imaging detectors can enter. Its high resolution and real-time imaging capability make it useful in some experiments. Examples are as follows.

(i) For adjustment of optical elements. The fast readout of the CMOS detectors makes it possible to observe reflected or scattered X-ray beams from optical devices with high sensitivity. The robustness of the detector also allows one to work with an intense beam.

(ii) For specimen adjustment. Fast readout is useful in positioning a specimen on the beam. The apparent sensitivity and frame rate may be increased by binning pixels. With C7942, 2×2 or 4×4 binning can be used and the frame rate increases twofold with 2×2 and fourfold with 4×4 binning. This is most useful when an image plate is the detector.

The CMOS technology is still rapidly developing. A CMOS imager with a larger area has been announced by Hamamatsu Photonics (C7930-01), which has an active area of 220×176 mm (4426×3520 pixels). Another improvement will be made on the readout circuit. Readout can be made faster by increasing the number of amplifiers and A/D converters. For example, a higher frame rate can be achieved by simply increasing the number of segments in C7942. In an ultimate design, each line may have an amplifier and A/D converter. A possibility that has not yet been explored is random readout. Since a CMOS photodiode array is read by column–row addressing, in principle it is possible to read only the pixels that are necessary for the purpose of the experiment. This will considerably reduce the readout time and increase the frame rate. Although this function has not been implemented, it will be a unique feature of CMOS imagers that is not achievable with the CCD.

We thank Drs K. Miura and N. Shimizu for help in the tests at BL38B1, which were made with the approval of the R&D Beamline Program Committee of SPring-8. We also thank Mr H. Mori of Hamamatsu Photonics KK for construction of the prototype detectors and for valuable discussions. Part of the results were obtained by funding to RIKEN in the RR2002 project of the Ministry of Education, Culture, Sports, Science and Technology, and by the SPring-8 Joint Research Promotion Scheme of the Japan Science and Technology Corporation.

References

- Amemiya, Y., Ito, K., Yagi, N., Asano, Y., Wakabayashi, K., Ueki, T. & Endo, T. (1995). *Rev. Sci. Instrum.* **66**, 2290–2294.
- Coltman, J. W. (1954). *J. Opt. Soc. Am.* **44**, 468–471.
- Dorenzo, S. & Moses, W. (1993). *Heavy Scintillators for Scientific and Industrial Applications*, edited by F. De Notaristefani, P. Lecoq and M. Schneegans, pp. 125–135. France: Editions Frontieres.
- Goto, S., Takeshita, K., Suzuki, Y., Ohashi, H., Asano, Y., Kimura, H., Matsushita, T., Yagi, N., Isshiki, M., Yamazaki, H., Yoneda, Y., Umetani, K. & Ishikawa, T. (2001). *Nucl. Instrum. Methods*, **A467/468**, 682–685.
- Graeve, T. & Weckler, G. P. (2001). *Proc. SPIE*, **4320**, 68–76.
- Gruner, S. M. & Ealick, S. E. (1995). *Structure*, **3**, 13–15.
- Inoue, K., Oka, T., Suzuki, T., Yagi, N., Takeshita, K., Goto, S. & Ishikawa, T. (2001). *Nucl. Instrum. Methods*, **A467/468**, 674–677.
- Koch, A., Raven, C., Spanne, P. & Snigirev, A. (1998). *J. Opt. Soc. Am.* **A15**, 1940–1951.
- Pflugrath, J. W. (1999). *Acta Cryst.* **D55**, 1718–1725.
- Tate, M. W., Gruner, S. M. & Eikenberry, E. F. (1997). *Rev. Sci. Instrum.* **68**, 47–54.
- Uesugi, K., Suzuki, Y., Yagi, N., Tsuchiyama, A. & Nakano, T. (2001). *Nucl. Instrum. Methods*, **A467/468**, 853–856.
- Yagi, N., Suzuki, Y., Umetani, K., Kohmura, Y. & Yamasaki, K. (1999). *Med. Phys.* **26**, 2190–2193.
- Yagi, N., Yamamoto, M., Uesugi, K. & Inoue, K. (2004). *Proceedings of the Eight International Conference on Synchrotron Radiation Instrumentation*, pp. 885–888. New York: AIP.